Metal-Organic Framework Mixed-Matrix Coatings on 3D Printed Devices

Andreu Figuerola[1], Deyber A.V. Medina[1,2], Alvaro J. Santos-Neto[2], Carlos Palomino Cabello[1], Víctor Cerdà[1], Gemma Turnes Palomino*[,1], Fernando Maya*[,1,3]

[1]*University of the Balearic Islands. Cra Valldemossa km 7.5, Palma de Mallorca, E-07122, Spain.*

[2]*Sao Carlos Institute of Chemistry, University of Sao Paulo, 13566-590, Sao Carlos, SP, Brazil.*

[3]*Australian Centre for Research on Separation Science (ACROSS), School of Natural Sciences-Chemistry, University of Tasmania, Private Bag 75, Hobart, TAS, 7001, Australia.*

Corresponding author: fernando.mayaalejandro@utas.edu.au, g.turnes@uib.es

Abstract

Strategies to incorporate porous coatings on 3D printed devices with intricate geometries are critical to expanding the scope of application of this type of manufacturing technique. Herein, the preparation of metal-organic framework (MOF)/polymer dispersions to be applied as coatings for 3D printed devices is described. As a proof of concept, submicrometric crystals of a zeolitic imidazolate framework (ZIF-67) were dispersed in a binary mixture comprising a polymer and an organic solvent. The resulting dispersion is dispensed through the structure of 3D printed devices, and after gentle heating for a short time, a homogeneous and robust MOF/polymer mixed-matrix coating (MMC) is formed on the effective area of the 3D printed device. The developed MOF-MMC procedure is simple, fast, and does not require specific instrumentation, or synthetic skills. The resulting MOF-MMC 3D printed devices were evaluated for the peroxymonosulfate activation to enhance the degradation of organic dyes in water. After a degradation time of 30 min using rhodamine B (5 mg L^{-1}) as a model dye,

the MOF-MMC 3D printed devices showed excellent reusability and reproducibility, degrading an average of 97-98% of the rhodamine B after 10 consecutive degradation cycles comparing three different devices. Dye degradation was evaluated in stirred-tank and flow-through column formats, demonstrating that the developed MOF-MMC procedure is a versatile, safe and convenient way to implement micro/nanoparticulated materials for water pollutant degradation applications.

Keywords: 3D printing; metal-organic frameworks; mixed-matrix coating; peroxymonosulfate activation; environmental catalysis

1. Introduction

Additive manufacturing (3D printing) is revolutionizing many fields such as medicine [1], synthetic chemistry [2], pharmaceutical production [3], energy [4], catalysis [5], microfluidics [6], sensor fabrication [7, 8], or the development of novel analytical technologies [9, 10]. The search for 3D printable materials with improved features is an active field of research [11]. However, the small surface area of polymer-based 3D printable materials is one of the current bottlenecks to further expand the scope of application of 3D printing.

Metal-organic frameworks (MOFs) are an interesting class of advanced porous materials based on the coordination of metal centers with organic rigid linkers, resulting in porous materials that exhibit very high surface areas [12–14]. Among their different applications [14], MOFs are becoming promising materials for pollutant extraction and degradation [15–18].

The development of novel approaches to incorporate MOFs in 3D printed devices is gaining interest [19-26]. Recent progress has been made by incorporating MOFs in 3D printed scaffolds by using extrusion-based printers [19-22]. These approaches rely on MOF

incorporation in acrylonitrile butadiene styrene filaments [19], the use of MOF-bentonite clay-poly(vinyl alcohol) extrudable pastes [20], the preparation of MOF-based extrudable inks using Pluronic F127 [21], or the preparation of hybrid hydrogels based on MOF anchored on oxidized cellulose nanofibers [22]. MOFs have been also dispersed in 3D printable resins, followed by MOF embedding using Digital Light Processing techniques [23]. The embedding of the MOF crystals in the 3D printed polymer support, which generally takes place when using the above mentioned procedures to incorporate MOFs to 3D printed devices, was circumvented by the post-printing partial dissolution of the 3D printed polymer in an appropriate organic solvent, which allows to expose part of the initially obstructed micropores of the embedded MOF [24]. Alternatively, MOFs have been in situ grown by a post 3D printing layer-by-layer approach on already preformed 3D printed devices [25, 26], or attached on the surface of partially fused polymer particles, by using Selective Laser Sintering, remaining accessible to fluids passing through the 3D printed device [27]. However, approaches to coat just the effective area of 3D printed devices in a fast and efficient way have not been reported to date. Such approach would be desirable to incorporate porous coatings on intricate 3D printed devices with a large size, such as integrated packings [28, 29], or membranes [30, 31]. Recent efforts to position functional materials on the effective surface of 3D printed devices include the immobilization of polyoxometalates via polymer surface modification for water decontamination [32], or the direct immobilization of sorbents into stereolithography (SLA) 3D printed devices in the "green state" [33, 34]. With the latter approach, 3D printed supports for the removal of dyes from water using hyperporous carbons [33], and the extraction of radionuclides by immobilized selective beads [34], have been accomplished. However, these approaches rely on time-consuming surface modification procedures, or they are limited to small sized and accessible 3D printed structures.

The aim of this work is to develop a simple and efficient post-printing approach to coat 3D printed devices based on intricate geometries with microporous materials. To

achieve our goal, we explored the use of MOF dispersions in polymer/solvent mixtures typically used for the preparation of mixed-matrix membranes [35], reaching in this way the whole effective area of the 3D printed device. To the authors' knowledge, the potential of mixed-matrix precursors as coatings for 3D printed devices has not been explored yet. As a proof-of-concept, we have tested the immobilization of submicrometric crystals of the zeolitic imidazolate framework (ZIF-67) [36], onto SLA 3D printed devices via dispersion in polyvinylidene fluoride/dimethylformamide (PVDF/DMF) mixtures obtaining a MOF-mixed-matrix coated (MOF-MMC) 3D printed devices. The so prepared coated devices have been evaluated for the activation of potassium peroxymonosulfate (PMS) to form sulfate radicals [37], which are strong oxidants capable to degrade organic synthetic dyes from water [38], whose presence is a concern in industrial areas [39]. In addition, the fabricated MOF-MMC 3D printed devices have been evaluated for the degradation of dye pollutants in both stirred batch mode and flow-through column format.

2. MATERIALS AND METHODS

2.1. Materials

2-methylimidazole (2-MIM) (99%), rhodamine B (95%), malachite green oxalate (95%), polyvinylidene fluoride (PVDF, MW ~ 180,000), cobalt nitrate hexahydrate ($Co(NO_3)_2{\cdot}6H_2O$) (98%), methyl orange (85%), methylene blue (95%), and potassium peroxymonosulfate (PMS, OXONE®), were purchased from Sigma-Aldrich. Dimethylformamide (DMF) (99.5%), methanol (99.8%), and 2-propanol (synthesis grade) were purchased from Scharlab. All chemicals were used as received without any further purification. Ultrapure water (18.2 MΩ cm) was obtained from a Milli-Q water generator.

2.2. Instrumentation

A Formlabs Form 2 3D Printer and clear photoactive resin (Formlabs Clear V4 (FLGPCL04)), composed by methacrylate monomers/oligomers and an initiator, were used for device fabrication. An Upland CL-1000 ultraviolet crosslinker with a 365 nm UV lamp was used for post-curing the 3D printed devices. Powder X-ray diffraction (PXRD) and micro X-ray microdiffraction (μXRD) patterns were obtained using Cu Kα radiation on a Bruker D8 Advance diffractometer. Scanning Electron Microscopy (SEM) was carried out using a Hitachi S-3400N microscope. Nitrogen adsorption–desorption isotherms were measured at 77 K using a TriStar II (Micromeritics) gas adsorption analyzer. The samples were previously outgassed at 393 K overnight. Data were analyzed by using the Brunauer-Emmett-Teller model (BET) to determine the specific surface area. The proper experimental range of relative pressures to apply the BET model was determined following the procedure described by Rouquerol et al [40]. Absorbance measurements were carried out using a HP 8453 UV-Vis spectrophotometer.

2.3. Fabrication of 3D printed devices

The design of the 3D printed devices was carried out using the software Rhinoceros 5.0 SR11 32 (McNeel & Associates, USA). The STL files for the 3D printed devices used in this work are shared in the Supporting Information. The printing time for the basic device based on a matrix of interconnected cubes (Figure 1a) was 50 min. However, up to 21 devices were 3D printed simultaneously in just 119 min. These devices were 3D printed vertically with stand with a resolution of 0.100 mm and 141 layers. Its weight was 100 mg, and just 0.88 ml of resin were required per device, with an approximate cost of 0.13 USD. The 3D printed devices were rinsed thoroughly with 2-propanol to remove unreacted monomers, followed by drying at room temperature. UV post-curing was carried out for 4 h at 365 nm.

2.4. Preparation of ZIF-67

ZIF-67 was synthesized according a procedure previously reported in the literature with minor modifications [41]. Briefly, a solution of 4 mmol of $Co(NO_3)_2 \cdot 6H_2O$ in 100 ml of methanol was slowly poured into another one of 16 mmol of 2-MIM in 100 ml of methanol. The resulting mixture was stirred at room temperature for 2 h. The resulting violet solid was collected by centrifugation and washed repeatedly with ethanol. The obtained crystals were dried at 60 °C in a conventional oven for 6 h. The yield of the final product was ~75% based on the amount of Co(II) added in the synthesis.

2.5. Immobilization of ZIF-67 in 3D printed devices

The preparation of ZIF-67/PVDF dispersions was carried out following the procedure reported by Denny and Cohen with minor modifications [35]. ZIF-67 crystals (150 mg) were dispersed in 5 ml of acetone by sonicating for 30 min. The so prepared dispersion was mixed with 1 g of a PVDF solution (7.5 wt% in DMF) to obtain a ratio of ZIF-67:PVDF of 2:1 (w:w). The resulting mixture was then sonicated for 30 minutes, followed by acetone evaporation under a gentle nitrogen flow, obtaining a ZIF-67 dispersion in PVDF/DMF, which was added dropwise (dip-coated, or pumped) onto the 3D printed device (Figure 1b). After removing the excess of the dispersion by using a gentle nitrogen stream, the 3D printed device coated with the ZIF-67 dispersion was placed in a convection oven at 60°C for 1 h for DMF evaporation. Finally, the resulting ZIF-67-MMC 3D printed device was rinsed thoroughly with 2-propanol observing no leaching of ZIF-67 particles from the device.

2.6. 3D printed device for dye degradation in stirred batch-mode

In order to use the 3D printed device for extraction in stirred batch-mode, a thin metallic wire (0.5 mm diameter, 17.60 mm length) was inserted through the cube interspaces of the 3D

printed device. The desired volume of the aqueous dye solution was added to a 250 ml beaker together with the 3D printed device. The solution was stirred for the desired amount of time using a stirring plate. Since the ZIF-67 crystals are immobilized onto the 3D printed device, different aliquots can be taken from the solution and directly measured by UV-vis spectrophotometry with no need to filter, or centrifugate the solution. After dye degradation, the 3D printed device was easily retrieved from the aqueous solution using a magnetic stir bar and rinsed with Milli-Q water before reuse.

2.7. 3D printed device for dye degradation in flow through column format

In the case of the 3D printed column-based flow-through device with integrated packing, the column was connected to a multisyringe pump equipped with 2 x 5 ml glass syringes. Syringe 1 contained an aqueous organic dye solution and Syringe 2 contained the PMS solution. Each syringe was connected to a 2-way solenoid valve. The first position of the solenoid valve was connected to a rhodamine B, or PMS, reservoirs enabling the automatic syringe refilling. The second position of the solenoid valves were connected to the two inlets of the column-based 3D printed device. The outlet of the 3D printed column was directly connected to a UV-vis spectrophotometer using a 1-cm optical pathlength flow cell. Rhodamine B absorbance was monitored at 553 nm.

3. RESULTS AND DISCUSSION

3.1. Incorporation of ZIF-67 mixed-matrix coating on 3D printed devices

As starting point, we carried out the synthesis of ZIF-67 following a mild and high yield synthetic procedure at room temperature, obtaining submicrometric microporous ZIF-67 crystals with a surface area of 1369 m^2g^{-1} (Supporting Information, Figure S1 and Figure S2). A 3D printed device based on a matrix of interconnected cubes with a diameter of 8 mm and a height of 5.5 mm was then 3D printed using the SLA technique. Figure 1a shows the

design of the basic 3D printed device from top and front views and a SEM image of the surface of a cube located in one of the edges of the device. The different layers of 3D printed polymer used for the fabrication of the cube can be clearly observed in the SEM image, as well as the typical smooth surface of the 3D printed device fabricated by SLA. A scheme of the developed procedure to coat the 3D printed device is shown in Figure 1b. The coating procedure is simple, fast, and no specialized instrumentation is required. In the first step, approximately 1 h is required to obtain the dispersion of ZIF-67 in PVDF/DMF. After that, the resulting dispersion is simply added to the 3D printed device, and after removing the excess of ZIF-67 dispersion, this one becomes permanently immobilized after heating for 1 h at 60^{o}C. The mechanism of the ZIF-67 coating relies on the solubilization-precipitation of PVDF in the presence/absence of DMF. Pellets of PVDF are dissolved in DMF obtaining a stable solution miscible with a ZIF-67/acetone dispersion, which after acetone removal results in a dense and stable ZIF-67/PVDF/DMF dispersion. The final dispersion is well retained on the surface of acrylate-based 3D printed devices by dip-coating, or by pumping the dispersion through the channels of the 3D printed device. By gentle heating of the coated 3D printed device, DMF is slowly evaporated, becoming the dispersion rich in PVDF. The phase separation of PVDF is produced, reprecipitating on the surface of the 3D printed device entrapping the ZIF-67 crystals and obtaining a permanent MMC covering the entire effective surface of the 3D printed device. Figure 1b also shows a SEM image of a MOF-MMC 3D printed device. It can be observed that, after coating, the surface of the device is fully covered with submicrometric ZIF-67 crystals becoming rough, although the layers of the 3D printed material can still be noticed.

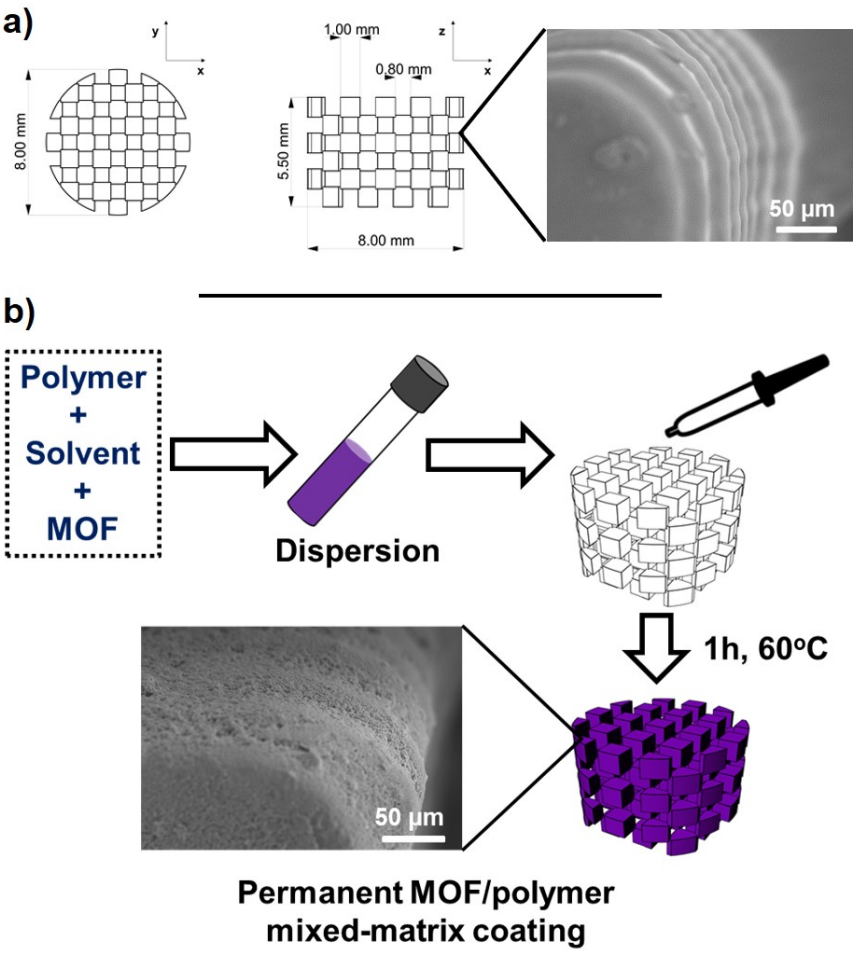

Figure 1. a) Top and front views of the design of the basic 3D printed device. b) Schematic representation of the developed method for immobilizing MOF mixed-matrix coatings on 3D printed devices together with a SEM micrograph of the coated device.

To study the reproducibility of the developed coating procedure, 10 replicates of the device shown in Figure 1a were 3D printed and coated with the same ZIF-67 dispersion. The average weight of the MOF-MMC after subtracting the weight of the 3D printed polymer scaffold (100 mg) was 29.6±3.7 mg, representing a device-to-device variation of the amount of MOF-MMC of a 12.5 wt% (RSD, n= 10). Figure 2a shows the morphology of the cube-based structure of an uncoated 3D printed device. Magnified images of a cube of the uncoated 3D printed device and a detail of its smooth surface are shown in Figure 2b and Figure 2c, respectively. Figure 2d shows a SEM image of a cube of the MOF-MMC device

after applying the developed coating method, where it can be observed a uniform coating covering entirely the surface of the cube. A magnified image of the surface of a coated cube (Figure 2e) shows the homogeneous and dense packing of the ZIF-67 crystals. A closer view of the MOF-MMC device shows clearly the presence of the PVDF polymer matrix entrapping the submicrometric ZIF-67 crystals (Figure S3). To gain insight into the thickness of the MOF-MMC, a square rod of 1 mm width and 10 mm length was 3D printed, and subsequently coated. A SEM image of the cross-section of the coated 3D printed rod shows that the thickness of the coating is 30 μm (Figure 2f), approximately.

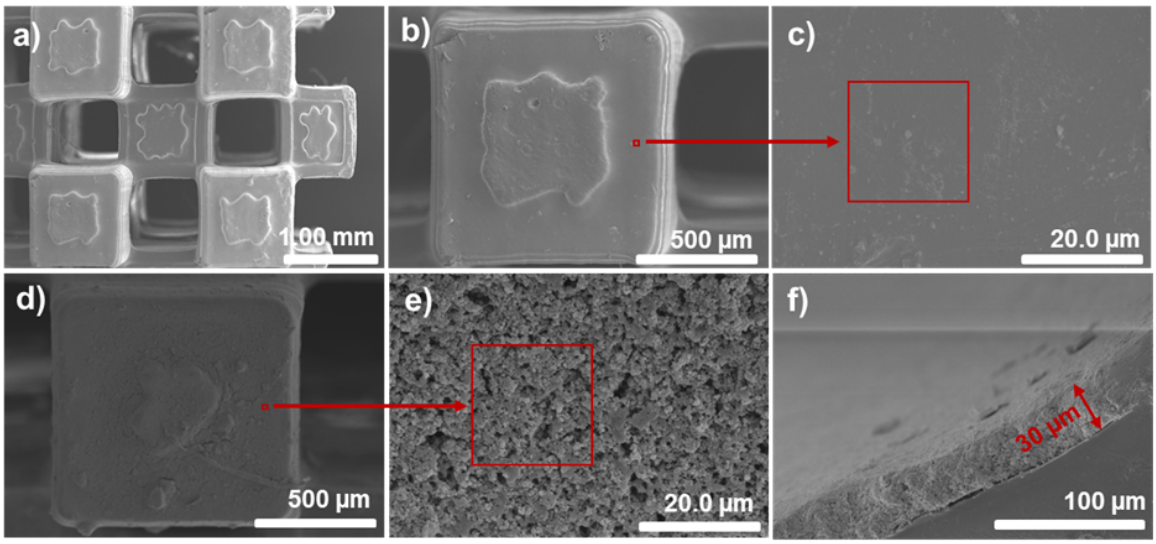

Figure 2. SEM images of 3D printed devices: a-c) Uncoated 3D printed device at different magnification. d-e) MOF-MMC 3D printed device at different magnification. f) Cross-section image of a cube of a MOF-MMC 3D printed device.

Figure 3a shows the XRD pattern of the as-synthesized ZIF-67 crystals together with the μXRD pattern (obtained from the selected areas shown in Figures 3b and 3c) of a 3D printed device before and after coating with the MOF-MMC. Before coating, the XRD pattern just shows a broad band corresponding to the amorphous uncoated 3D printed polymer, while the most intense diffraction bands present in the ZIF-67 diffractogram are also clearly visible in the μXRD pattern of the coated device. The μXRD experiment was repeated at 3 different

locations of a MOF-MMC 3D printed device detecting in all instances the presence of ZIF-67 diffraction peaks as shown in Figure 3d, demonstrating the homogenous distribution of the ZIF-67 crystals on the surface of the MOF-MMC device.

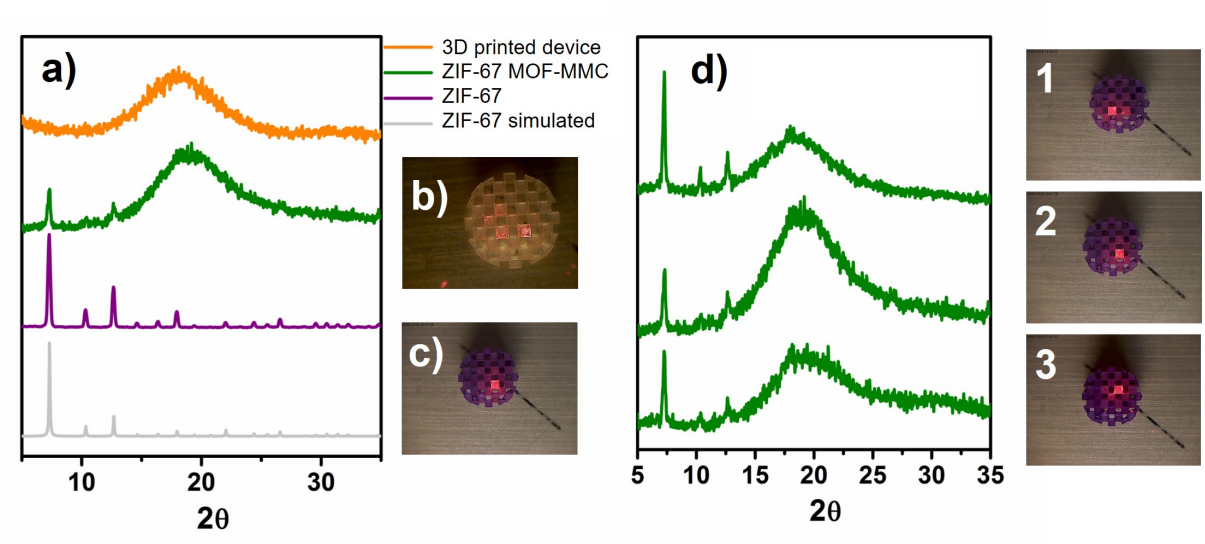

Figure 3. Simulated XRD pattern of ZIF-67, XRD pattern of the as-synthesized ZIF-67 crystals, and μXRD patterns of a 3D printed device before and after coating with a MOF-MMC (a). Images of the uncoated (b) and MOF-MMC (c) 3D printed devices showing the area analyzed by μXRD. Comparison of the μXRD patterns of three different spots of a MOF-MMC 3D printed device (d).

3.2. Degradation of rhodamine B in water

Porous crystalline MOFs are promising materials for the highly efficient extraction of pollutants from water [42], including organic dyes [43], heavy metals [44], or both families of pollutants simultaneously [45]. In addition, certain MOFs such as ZIF-67, have also shown promising results as catalysts for the degradation of pollutants from water [37, 46]. To test the efficiency for the degradation of organic pollutants of the prepared MOF-MMC 3D printed devices, the oxidation of the rhodamine B dye in water was selected as model experiment. A basic 3D printed device, as that shown in Figure 1b, was stirred in an aqueous solution of

252 rhodamine B in the presence of PMS. As shown in Figure 4, just 10 minutes were required to
253 completely degrade the rhodamine B solution under the selected experimental conditions,
254 observing no trace of the dye remaining after degradation (Figure S4). This result was
255 compared with the same experiment using an uncoated 3D printed device and dispersing
256 the ZIF-67 crystals in the solution. In this case, just 5 min were required to completely
257 degrade the rhodamine B (Figure 4), but a laborious and time-consuming centrifugation
258 process was needed to completely remove the submicrometric ZIF-67 crystals dispersed in
259 the aqueous medium, which is a critical step to recover the catalyst enabling the safe reuse
260 of the purified water. However, when the ZIF-67 was immobilized onto the 3D printed device,
261 it was easily retrieved from the aqueous medium by using an external magnet in a simple
262 and safe manner, leaving no free ZIF-67 crystals in the medium. In the absence of PMS
263 (Figure 4), the MOF-MMC 3D printed device just removed a 4% of the rhodamine B after 30
264 min, which is attributed to the dye adsorption on the coated 3D printed device. In a similar
265 experiment, in this case in the absence of ZIF-67 (Figure 4), the PVDF coated 3D printed
266 device just removed a 10% of the rhodamine B, attributed to the dye adsorption on the
267 PVDF coating and the polymer of the 3D printed device, as well as the possible dye
268 degradation by the PMS present in the medium.

269

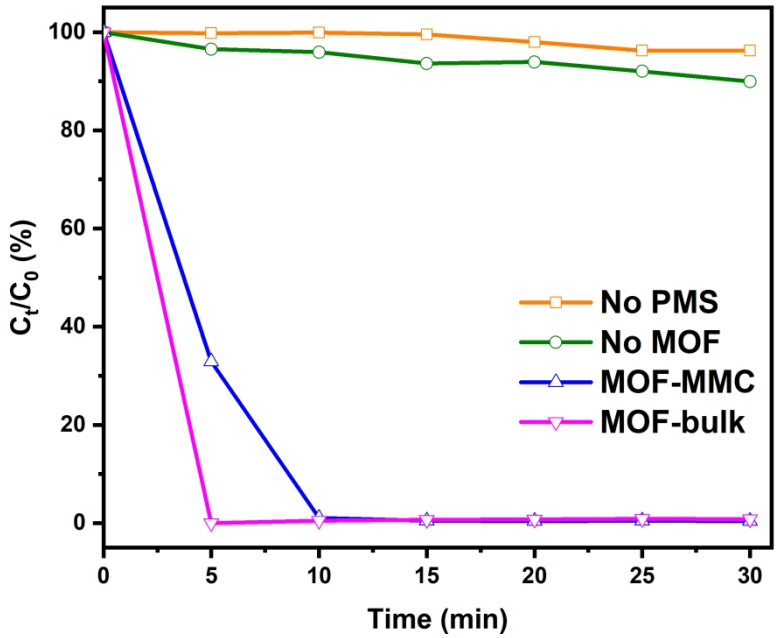

Figure 4. Elimination of rhodamine B based on PMS activation using the ZIF-67-based MOF-MMC 3D printed device. Comparison with rhodamine B degradation using the MOF-MMC 3D printed device in the absence of PMS, absence of MOF, and using an uncoated 3D printed device stirring freely dispersed ZIF-67 crystals (20 mg) in the rhodamine B solution (MOF-bulk). 3D printed devices were stirred at 200 rpm. Weight of added PMS, 20 mg. Volume of rhodamine B solution, 100 ml. Concentration of rhodamine B solution, 5 mg L^{-1}.

3.3. Reusability of the 3D printed devices

As the reusability of an adsorbent is a crucial factor from the practical application point of view, the XRD of ZIF-67 was recorded again after rhodamine B degradation (Figure S5), showing that the crystals structure of the ZIF-67 catalyst was preserved.

To ensure the regenerability and the reusability of the MOF-MMC 3D printed devices, the rhodamine B degradation was repeated 10 consecutive times (Figure 5). Three different MOF-MMC 3D printed devices were satisfactorily reused for at least 10 rhodamine B degradation cycles obtaining an excellent reproducibility. Variations of just a 1.4%, 1.6%, and 2.1% (expressed as RSD, %) were obtained for the three different devices. Besides,

once the activity began to decrease, the developed MOF-MMC 3D printed devices are potentially and easily recyclable since the MOF-based coating can be dissolved in acidic aqueous medium and renewed by applying a new coating cycle with a ZIF-67/PVDF/DMF dispersion.

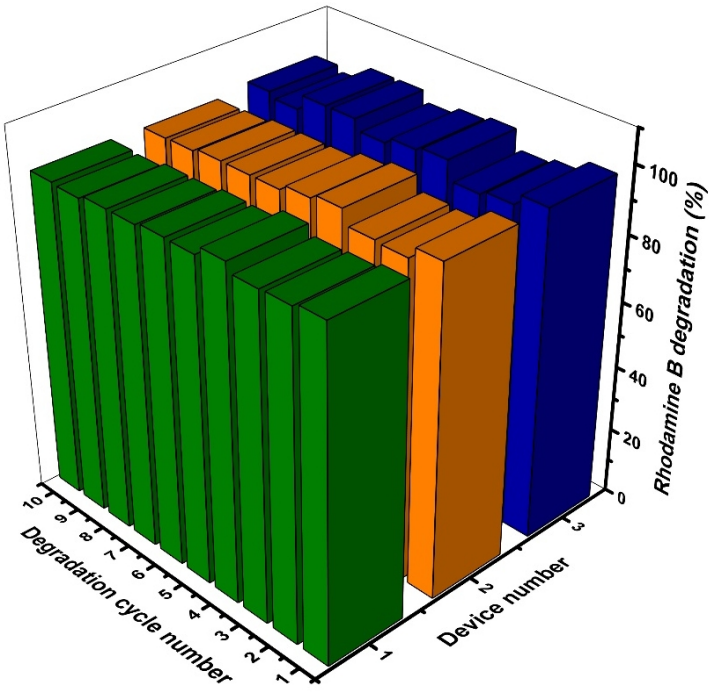

Figure 5. Reusability for 10 consecutive catalytic degradation cycles of rhodamine B using three different MOF-MMC 3D printed devices. Rhodamine B concentration, 5 mg L^{-1}. Stirring rate, 200 rpm. Extraction time, 30 min.

3.4. Degradation of other organic dyes

The efficiency of the MOF-MMC 3D printed devices for the degradation of rhodamine B was compared with that of other organic dyes. A similar degradation performance for malachite green, methylene blue and methyl orange was obtained when compared with the degradation of rhodamine B (Figure 6). In all instances, just 10 minutes were required for the complete degradation of the selected organic dyes.

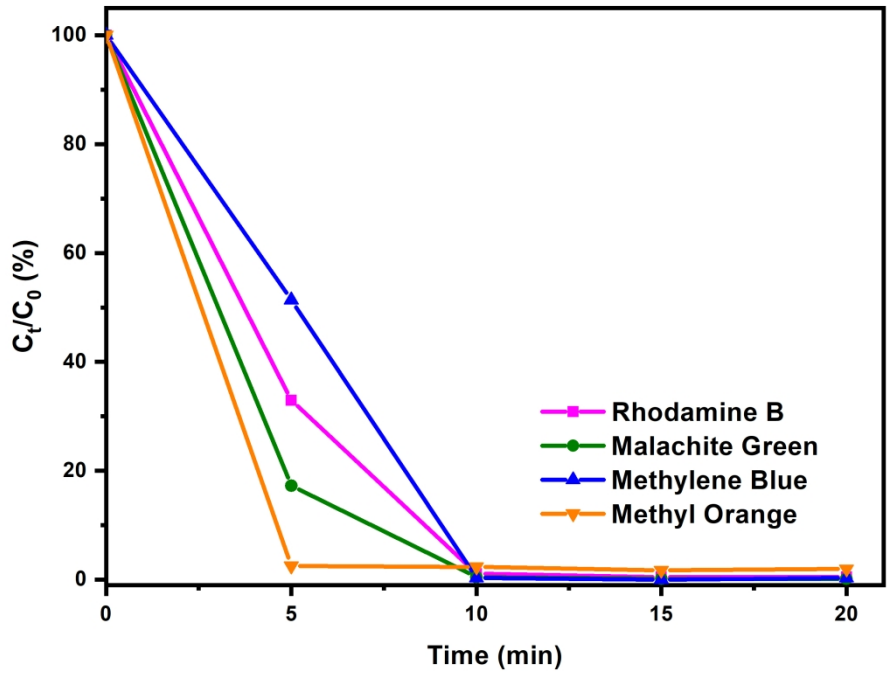

Figure 6. Elimination of different pollutant dyes from water using a MOF-MMC 3D printed device. PMS, 20 mg L^{-1}; dye concentration, 5 mg·L^{-1}. Stirring rate, 200 rpm.

3.5. Degradation of rhodamine B in flow-through format

The basic 3D design based on a matrix of small interconnected cubes (Figure 1a) was adapted to an integrated packing in column format. The design of the 3D printed column is shown in Figure 7a, and the corresponding STL file is shared in the Supporting Information. The 3D printed column was filled with the same dispersion of ZIF-67/PVDF/DMF used for coating the 3D printed cubes with the aid of a disposable syringe. After removing the excess of dispersion by passing a gentle nitrogen stream through it, the column with the inlets/outlet opened was placed inside a conventional oven for 1 h at 60ºC. Finally, unreacted monomers were removed by rinsing with 2-propanol. Once coated, Rhodamine B and PMS solutions were pumped through the two inlets of the column using a multi-syringe pump. The outlet of the column was connected to a flow cell with 1 cm optical pathlength for the continuous spectrophotometric monitoring of the rhodamine B absorbance.

318 Pumping the rhodamine B and the PMS solutions at 1 ml min^{-1}, resulted in a total
319 flow rate of 2 ml min^{-1} through the MOF-MMC, ensuring enough residence time to
320 completely degrade a 5 mg L^{-1} rhodamine B solution (Figure 7b). The system was left to
321 continuously operate refilling automatically the syringes (5 ml volume) with the rhodamine B
322 and PMS solutions. At this flow rate, no rhodamine B was detected in the effluent of the
323 column until pumped a volume of 500 ml of rhodamine B solution through the column, when
324 a small amount of non-degraded (<0.5 mg L^{-1}) rhodamine B was noticed. The flow rate
325 through the 3D printed column was increased up to 20 ml min^{-1}, noticing no overpressure
326 thanks to the 3D printed cubes are sufficiently separated to allow a high-water permeability
327 through the support. However, as shown in Figure 7b, the rhodamine B breakthrough
328 increased by increasing the flow rate, from 0% using a flow rate of 2 ml min^{-1}, to almost an
329 80% by increasing the flow rate to 20 ml min^{-1}. Further optimization of column dimensions,
330 packing design, or the use of 3D printers with improved resolution will probably lead to
331 exciting developments on catalytic and separation media for synthetic, analytical, or
332 environmental applications. In addition, the developed coating method open new avenues
333 for the study of other types of MOFs for flow-based applications, as for instance
334 photoluminescent MOFs to create integrated sensors in 3D printed devices [47], or for the
335 immobilization of other types of materials for pollutant degradation, such as metal oxide
336 nanosheets [48].

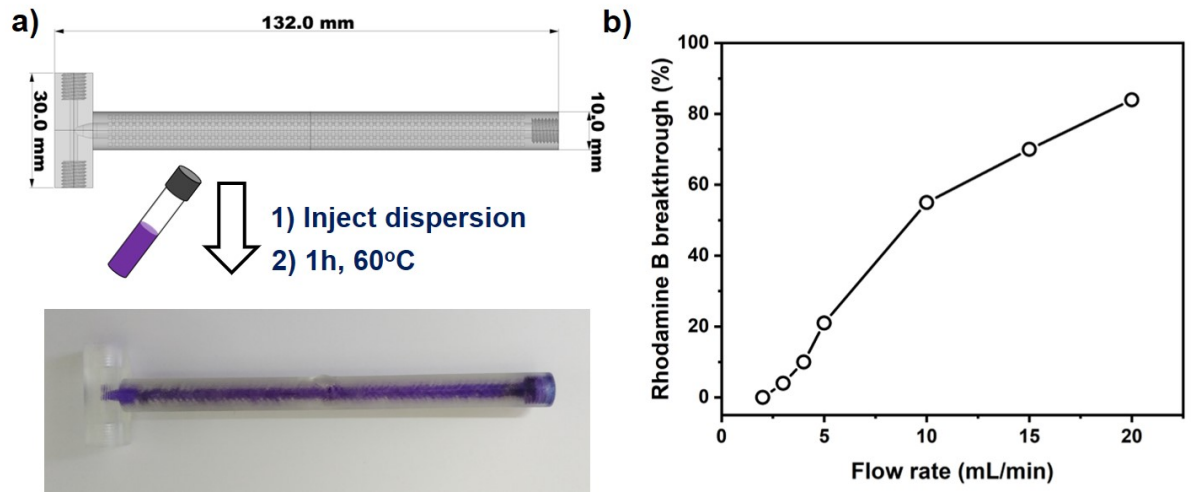

Figure 7. a) Design of the 3D printed column with integrated packing based on interconnected cubes and picture of the column with the MOF-MMC. b) Effect of flow rate on the flow-based degradation of rhodamine B (5 mg L^{-1}) using the column shown in a).

4. CONCLUSIONS

Incorporation of submicrometric crystals of the metal-organic framework ZIF-67 on intricate 3D printed devices fabricated by stereolithography has been achieved via the use of PVDF as binder. The resulting ZIF-67 mixed-matrix coatings have been efficiently applied to coat 3D printed packings based on interconnected cube matrices. The incorporation of such coatings in flow-through devices in column format was also achieved in a simple and efficient manner, without requiring of specialized instrumentation. The developed MOF-MMC 3D printed devices showed high efficiency for the fast removal of rhodamine B from water by PMS activation. The fabricated devices were highly reproducible and reusable for the efficient degradation of different organic dyes from water in stirred and column-based formats. Future developments towards the use of robust materials for 3D printing and improvements on printing resolution can lead to interesting applications using MOF-MMCs for separation and catalysis, both in batch and flow modes. In addition, in-depth studies

357 towards the long-term stability and durability of 3D printed materials and immobilized
358 catalysts will be of a great interest for the practical real-life application of coated 3D printed
359 devices for water purification.

360

361 **ACKNOWLEDGEMENTS**

362 Spanish Agencia Estatal de Investigación (AEI) and the European Funds for Regional
363 Development (FEDER) are gratefully acknowledged for financial support through Project
364 CTQ2016–77155-R. A.F. thanks the Spanish Servicio Público de Empleo Estatal and
365 European Social Funds for financial support thorough Program SOIB Jove-Qualificats Sector
366 Públic. F.M. thanks MINECO for a Juan de la Cierva- Incorporación Fellowship (IJCI-2015-
367 24059). A.J.S.N and D.A.V.M. acknowledge the financial support from the São Paulo
368 Research Foundation (FAPESP), grant #2010/19910-9, grant #2014/03795-0, grant
369 #2016/21950-5, and grant #2017/02147. The authors acknowledge F. Hierro Riu for
370 scanning micrographs.

371

REFERENCES

[1] M.H. Michalski, J.S. Ross, The shape of things to come: 3d printing in medicine, JAMA 312 (2014) 2213–2214. https://dx.doi.org/10.1001/jama.2014.9542.

[2] M.D. Symes, P.J. Kitson, J. Yan, C.J. Richmond, G.J.T. Cooper, R.W. Bowman, T. Vilbrandt, L. Cronin, Integrated 3D-printed reactionware for chemical synthesis and analysis, Nat. Chem. 4 (2012) 349–354. https://doi.org/10.1038/nchem.1313.

[3] S.J. Trenfield, A. Awad, A. Goyanes, S. Gaisford, A.W. Basit, 3D printing pharmaceuticals: Drug development to frontline care, Trends Pharmacol. Sci. 39 (2018) 440–451. https://doi.org/10.1016/j.tips.2018.02.006.

[4] A. Ambrosi, M. Pumera, 3D-printing technologies for electrochemical applications, Chem. Soc. Rev. 45 (2016) 2740–2755. https://doi.org/10.1039/C5CS00714C.

[5] C. Parra-Cabrera, C. Achille, S. Kuhn, R. Ameloot, 3D printing in chemical engineering and catalytic technology: structured catalysts, mixers and reactors, Chem. Soc. Rev. 47 (2018) 209–230. https://doi.org/10.1039/C7CS00631D.

[6] S. Waheed, J.M. Cabot, N.P. Macdonald, T. Lewis, R.M. Guijt, B. Paull, M.C. Breadmore, 3D printed microfluidic devices: enablers and barriers, Lab Chip. 16 (2016) 1993–2013. https://doi.org/10.1039/C6LC00284F.

[7] E.H.Z. Ho, A. Ambrosi, M. Pumera, Additive manufacturing of electrochemical interfaces: Simultaneous detection of biomarkers, Appl. Mater. Today 12 (2018) 43–50. https://doi.org/10.1016/j.apmt.2018.03.008.

396 [8] T.S. Cheng, M.Z.M. Nasir, A. Ambrosi, M. Pumera, 3D-printed metal
397 electrodes for electrochemical detection of phenols, Appl. Mater. Today 9
398 (2017) 212–219. https://doi.org/10.1016/j.apmt.2017.07.005.

399 [9] E. Mattio, F. Robert-Peillard, L. Vassalo, C. Branger, A. Margaillan, C. Brach-
400 Papa, J. Knoery, J.-L. Boudenne, B. Coulomb, 3D-printed lab-on-valve for
401 fluorescent determination of cadmium and lead in water, Talanta 183 (2018)
402 201-208. https://doi.org/10.1016/j.talanta.2018.02.051.

403 [10] U. Kalsoom, P.N. Nesterenko, B. Paull, Current and future impact of 3D
404 printing on the separation sciences, Trends Anal. Chem. 105 (2018) 492–502.
405 https://doi.org/10.1016/j.trac.2018.06.006.

406 [11] J.-Y. Lee, J. An, C.K. Chua, Fundamentals and applications of 3D printing for
407 novel materials, Appl. Mater. Today 7 (2017) 120–133.
408 https://doi.org/10.1016/J.APMT.2017.02.004.

409 [12] H. Li, M. Eddaoudi, M. O'Keeffe, O.M. Yaghi, Design and synthesis of an
410 exceptionally stable and highly porous metal-organic framework, Nature. 402
411 (1999) 276–279. http://dx.doi.org/10.1038/46248.

412 [13] K.S. Park, Z. Ni, A.P. Côté, J.Y. Choi, R. Huang, F.J. Uribe-Romo, H.K. Chae,
413 M. O'Keeffe, O.M. Yaghi, Exceptional chemical and thermal stability of zeolitic
414 imidazolate frameworks, Proc. Natl. Acad. Sci. 103 (2006) 10186–10191.
415 https://doi.org/10.1073/pnas.0602439103.

416 [14] H. Furukawa, K.E. Cordova, M. O'Keeffe, O.M. Yaghi, The chemistry and
417 applications of metal-organic frameworks, Science 341 (2013) 1230444.
418 https://doi.org/10.1126/science.1230444.

[15] N.A. Khan, Z. Hasan, S.H. Jhung, Adsorptive removal of hazardous materials using metal-organic frameworks (MOFs): A review, J. Hazard. Mater. 244–245 (2013) 444–456. https://doi.org/10.1016/j.jhazmat.2012.11.011.

[16] C.-C. Wang, J.-R. Li, X.-L. Lv, Y.-Q. Zhang, G. Guo, Photocatalytic organic pollutants degradation in metal–organic frameworks, Energy Environ. Sci. 7 (2014) 2831–2867. https://doi.org/10.1039/C4EE01299B.

[17] P.A. Kobielska, A.J. Howarth, O.K. Farha, S. Nayak, Metal–organic frameworks for heavy metal removal from water, Coord. Chem. Rev. 358 (2018) 92–107. https://doi.org/10.1016/j.ccr.2017.12.010.

[18] Q. Gao, J. Xu, X.-H. Bu, Recent advances about metal–organic frameworks in the removal of pollutants from wastewater, Coord. Chem. Rev. 378 (2019) 17–31. https://doi.org/10.1016/j.ccr.2018.03.015.

[19] M.C. Kreider, M. Sefa, J.A. Fedchak, J. Scherschligt, M. Bible, B. Natarajan, N.N. Klimov, A.E. Miller, Z. Ahmed, M.R. Hartings, Toward 3D printed hydrogen storage materials made with ABS-MOF composites, Polym. Adv. Technol. 29 (2017) 867–873. https://doi.org/10.1002/pat.4197.

[20] H. Thakkar, S. Eastman, Q. Al-Naddaf, A.A. Rownaghi, F. Rezaei, 3D-printed metal–organic framework monoliths for gas adsorption processes, ACS Appl. Mater. Interfaces 9 (2017) 35908–35916. https://doi.org/10.1021/acsami.7b11626.

[21] Z. Lyu, G.J. Lim, R. Guo, Z. Kou, T. Wang, C. Guan, J. Ding, W. Chen, J. Wang, 3D-printed MOF-derived hierarchically porous frameworks for practical high-energy density Li–O_2 batteries. Adv. Func. Mater. 29 (2019) 1806658.

https://doi.org/10.1002/adfm.201806658.

[22] S. Sultan, H.N. Abdelhamid, X. Zou, A.J. Mathew, CelloMOF: nanocellulose enabled 3D printing of metal–organic frameworks. Adv. Funct. Mater. 29 (2019) 1805372. https://doi.org/10.1002/adfm.201805372.

[23] O. Halevi, J.M.R. Tan, P.S. Lee, S. Magdassi, Hydrolytically stable MOF in 3D-printed structures, Adv. Sustain. Syst. 2 (2017) 1700150. https://doi.org/10.1002/adsu.201700150.

[24] K. Evans, Z.C. Kennedy, B.W. Arey, J.F. Christ, H.T. Schaef, S.K. Nune, R.L. Erikson, Chemically-active, porous 3D-printed thermoplastic composites, ACS Appl. Mater. Interfaces 10 (2018) 15112–15121. https://doi.org/10.1021/acsami.7b17565.

[25] Z. Wang, J. Wang, M. Li, K. Sun, C. Liu, Three-dimensional printed acrylonitrile butadiene styrene framework coated with Cu-BTC metal-organic frameworks for the removal of methylene blue, Sci. Rep. 4 (2014) 5939. https://doi.org/10.1038/srep05939.

[26] Z. Shi, C. Xu, F. Chen, Y. Wang, L. Li, Q. Meng, R. Zhang, Renewable metal–organic-frameworks-coated 3D printing film for removal of malachite green, RSC Adv. 7 (2017) 49947–49952. https://doi.org/10.1039/C7RA10912A.

[27] E. Lahtinen, R.L.M. Precker, M. Lahtinen, E. Hey-Hawkins, M. Haukka, Selective laser sintering of metal‐organic frameworks: production of highly porous filters by 3D printing onto a polymeric matrix. ChemPlusChem 84 (2019) 222-225. https://doi.org/10.1002/cplu.201900081.

[28] C. Fee, S. Nawada, S. Dimartino, 3D printed porous media columns with fine

control of column packing morphology, J. Chromatogr. A. 1333 (2014) 18–24. https://doi.org/10.1016/j.chroma.2014.01.043.

[29] F. Dolamore, C. Fee, S. Dimartino, Modelling ordered packed beds of spheres: The importance of bed orientation and the influence of tortuosity on dispersion, J. Chromatogr. A. 1532 (2018) 150–160. https://doi.org/10.1016/j.chroma.2017.12.004.

[30] F. Li, P. Smejkal, N.P. Macdonald, R.M. Guijt, M.C. Breadmore, One-step fabrication of a microfluidic device with an integrated membrane and embedded reagents by multimaterial 3D printing, Anal. Chem. 89 (2017) 4701–4707. doi: 0.1021/acs.analchem.7b00409.

[31] U. Kalsoom, C.K. Hasan, L. Tedone, C. Desire, F. Li, M.C. Breadmore, P.N. Nesterenko, B. Paull, Low-cost passive sampling device with integrated porous membrane produced using multimaterial 3D printing, Anal. Chem. 90 (2018) 12081–12089. doi: 10.1021/acs.analchem.8b02893.

[32] Y. Ji, Y. Ma, Y. Ma, J. Asenbauer, S. Passerini, C. Streb, Water decontamination by polyoxometalate-functionalized 3D-printed hierarchical porous devices, Chem. Commun. 54 (2018) 3018–3021. https://doi.org/10.1039/C8CC00821C.

[33] D.A.V. Medina, A. Figuerola, F. Rodriguez, Á.J. Santos-Neto, C.P. Cabello, G.T. Palomino, V. Cerdà, F. Maya, Hyperporous carbon-coated 3D printed devices, Appl. Mater. Today 14 (2019) 29–34. https://doi.org/10.1016/J.APMT.2018.11.001.

[34] M.R. Ceballos, F.G. Serra, J.M. Estela, V. Cerdà, L. Ferrer, 3D printed resin-coated device for uranium (VI) extraction, Talanta 196 (2019) 510–514.

https://doi.org/10.1016/j.talanta.2018.12.055.

[35] M.S. Denny, S.M. Cohen, In situ modification of metal–organic frameworks in mixed‐matrix membranes. Angew. Chem. Int. Ed. 54 (2015) 9029-9032. https://doi.org/10.1002/anie.201504077.

[36] A.F. Gross, E. Sherman, J.J. Vajo, Aqueous room temperature synthesis of cobalt and zinc sodalite zeolitic imidizolate frameworks, Dalt. Trans. 41 (2012) 5458–5460. https://doi.org/10.1039/C2DT30174A.

[37] K.-Y.A. Lin, H.-A. Chang, Zeolitic Imidazole Framework-67 (ZIF-67) as a heterogeneous catalyst to activate peroxymonosulfate for degradation of Rhodamine B in water, J. Taiwan Inst. Chem. Eng. 53 (2015) 40–45. https://doi.org/10.1016/J.JTICE.2015.02.027.

[38] J. Wang, S. Wang, Activation of persulfate (PS) and peroxymonosulfate (PMS) and application for the degradation of emerging contaminants, Chem. Eng. J. 334 (2018) 1502–1517. https://doi.org/10.1016/j.cej.2017.11.059.

[39] M.T. Yagub, T.K. Sen, S. Afroze, H.M. Ang, Dye and its removal from aqueous solution by adsorption: A review, Adv. Colloid Interface Sci. 209 (2014) 172–184. https://doi.org/10.1016/j.cis.2014.04.002.

[40] J. Rouquerol, P. Llewellyn, F. Rouquerol, Is the bet equation applicable to microporous adsorbents?, in: P.L. Llewellyn, F. Rodriquez-Reinoso, J. Rouqerol, N.B.T.-S. in S.S. and C. Seaton (Eds.), Charact. Porous Solids VII, Elsevier, 2007: pp. 49–56. https://doi.org/10.1016/S0167-2991(07)80008-5.

[41] J. Shao, Z. Wan, H. Liu, H. Zheng, T. Gao, M. Shen, Q. Qu, H. Zheng, Metal

511 organic frameworks-derived Co_3O_4 hollow dodecahedrons with controllable
512 interiors as outstanding anodes for Li storage, J. Mater. Chem. A 2 (2014)
513 12194–12200. https://doi.org/10.1039/C4TA01966K.

514 [42] N.A. Khan, Z. Hasan, S.H. Jhung, Adsorptive removal of hazardous materials
515 using metal-organic frameworks (MOFs): a review. J Hazard Mater. 244 (2013)
516 444-456. https://doi.org/10.1016/j.jhazmat.2012.11.011.

517 [43] X.D. Du, C.C. Wang, J.G. Liu, X.D. Zhao, J. Zhong, Y.X. Li, J. Li, P. Wang,
518 Extensive and selective adsorption of ZIF-67 towards organic dyes:
519 performance and mechanism. J. Colloid Interface Sci. 506 (2017) 437-441.
520 https://doi.org/10.1016/j.jcis.2017.07.073.

521 [44] P.A. Kobielska, A.J. Howarth, O.K. Farha, S. Nayak, Metal–organic
522 frameworks for heavy metal removal from water. Coord. Chem. Rev. 358
523 (2018) 92-107. https://doi.org/10.1016/j.ccr.2017.12.010.

524 [45] Z. Shi, C. Xu, H. Guan, L. Li, L. Fan, Y. Wang, L. Liu, Q. Meng, R. Zhang,
525 Magnetic metal organic frameworks (MOFs) composite for removal of lead and
526 malachite green in wastewater. Colloids Surf. A 539 (2018) 382-390.
527 https://doi.org/10.1016/j.colsurfa.2017.12.043.

528 [46] D. Jiang, P. Xu, H. Wang, G. Zeng, D. Huang, M. Chen, C. Lai, C. Zhang, J.
529 Wan, W. Xue. Strategies to improve metal organic frameworks photocatalyst's
530 performance for degradation of organic pollutants. Coord. Chem. Rev. 376
531 (2018) 449-466. https://doi.org/10.1016/j.ccr.2018.08.005.

532 [47] H.E.Emam, H.N. Abdelhamid, R.M. Abdelhameed, Self-cleaned
533 photoluminescent viscose fabric incorporated lanthanide-organic framework
534 (Ln-MOF). Dyes Pigm. 159 (2018) 491-498.

https://doi.org/10.1016/j.dyepig.2018.07.026.

[48] A.S. Etman, H.N. Abdelhamid, Y. Yuan, L. Wang, X. Zou, J. Facile water-based strategy for synthesizing MoO_{3-x} nanosheets: efficient visible light photocatalysts for dye degradation. ACS omega 3 (2018) 2193-2201. DOI: 10.1021/acsomega.8b00012.

Supporting Information

Metal-Organic Framework Mixed-Matrix Coatings on 3D Printed Devices

Andreu Figuerola[1], Deyber A.V. Medina[1,2], Alvaro J. Santos-Neto[2], Carlos Palomino Cabello[1], Víctor Cerdà[1], Gemma Turnes Palomino*[,1], Fernando Maya*[,1,3]

[1]University of the Balearic Islands. Cra Valldemossa km 7.5, Palma de Mallorca, E-07122, Spain.

[2]Sao Carlos Institute of Chemistry, University of Sao Paulo, 13566-590, Sao Carlos, SP, Brazil.

[3]Australian Centre for Research on Separation Science (ACROSS), School of Natural Sciences-Chemistry, University of Tasmania, Private Bag 75, Hobart, TAS, 7001, Australia.

Corresponding author: fernando.mayaalejandro@utas.edu.au, g.turnes@uib.es

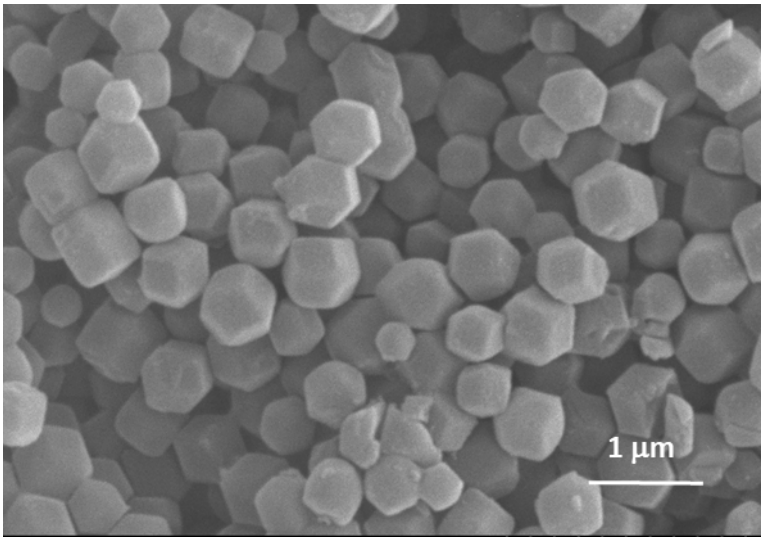

Figure S1. SEM image of the synthesized ZIF-67 crystals.

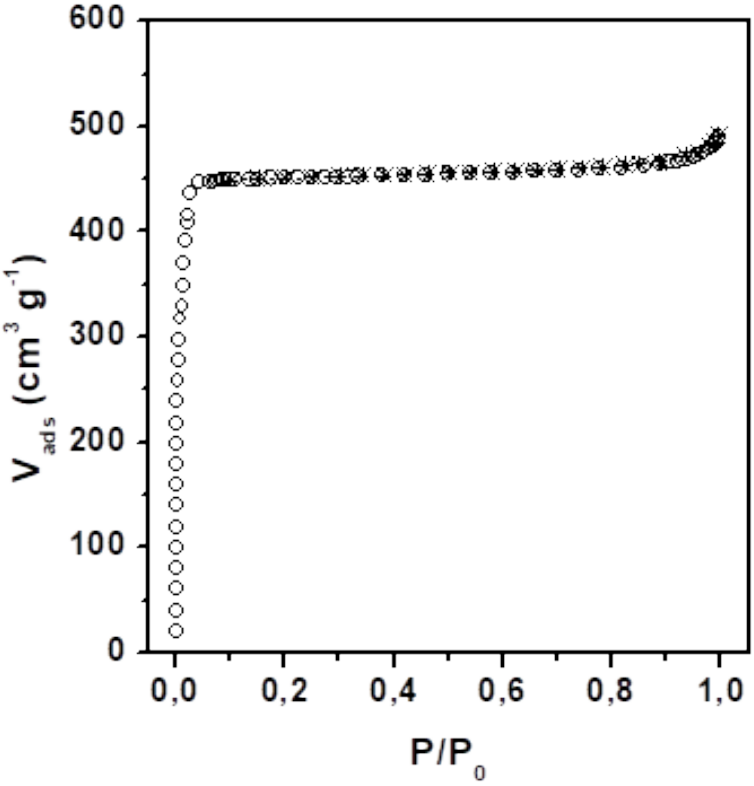

.

Figure S2. Nitrogen adsorption-desorption isotherms of the synthesized ZIF-67 crystals. BET surface area, 1369 m^2g^{-1}.

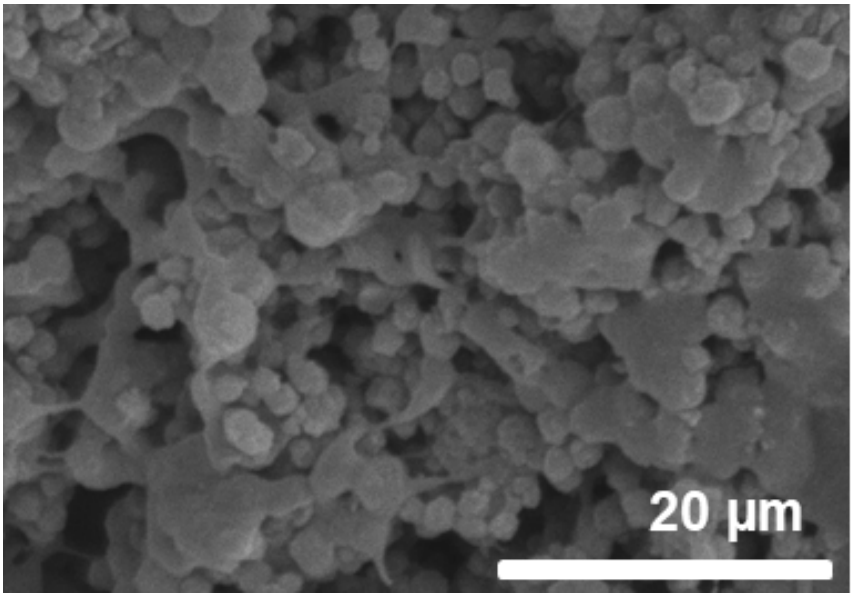

Figure S3. SEM image of a detail of a ZIF-MMC 3D printed device.

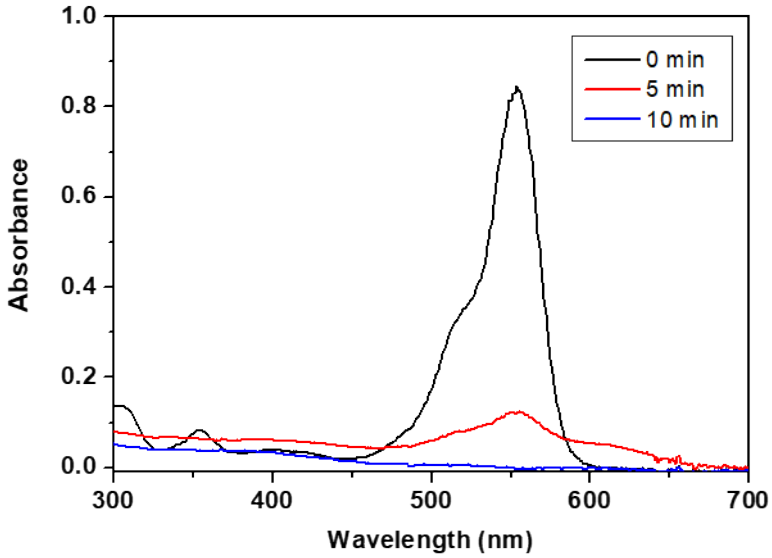

Figure S4. UV-Vis spectra for the degradation of rhodamine B with the ZIF-MMC 3D printed device. PMS, 20 mg L^{-1}; dye concentration, 5 mg·L^{-1}; stirring rate, 200 rpm.

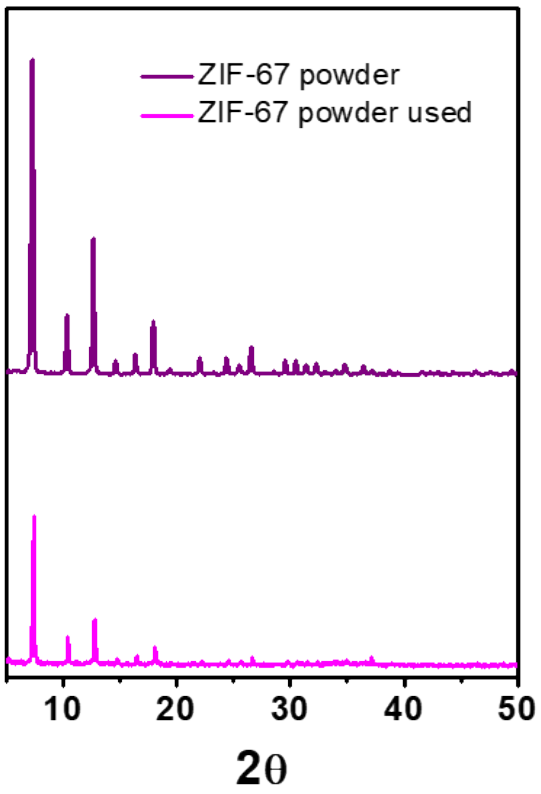

Figure S5. XRD of the ZIF-67 crystals before and after rhodamine B degradation.